JACS
JOURNAL OF THE AMERICAN CHEMICAL SOCIETY
Communication
pubs.acs.org/JACS

Light-Triggered, Self-Immolative Nucleic Acid-Drug Nanostructures

Xuyu Tan,[†] Ben B. Li,[§,∥] Xueguang Lu,[†] Fei Jia,[†] Clarissa Santori,[†] Priyanka Menon,[†] Hui Li,[‡] Bohan Zhang,[‡] Jean J. Zhao,[§,∥] and Ke Zhang*[,†,‡]

[†]Department of Chemistry and Chemical Biology, Northeastern University, Boston, Massachusetts 02115, United States
[‡]Institute of Chemical Biology and Nanomedicine, Hunan University, Changsha 410081, China
[§]Department of Cancer Biology, Dana Farber Cancer Institute, Boston, Massachusetts 02215, United States
[∥]Department of Biological Chemistry and Molecular Pharmacology, Harvard Medical School, Boston, Massachusetts 02215, United States

Supporting Information

ABSTRACT: The simultaneous intracellular delivery of multiple types of payloads, such as hydrophobic drugs and nucleic acids, typically requires complex carrier systems. Herein, we demonstrate a self-deliverable form of nucleic acid−drug nanostructure that is composed almost entirely of payload molecules. Upon light activation, the nanostructure sheds the nucleic acid shell, while the core, which consists of prodrug molecules, disintegrates via an irreversible self-immolative process, releasing free drug molecules and small molecule fragments. We demonstrate that the nanostructures exhibit enhanced stability against DNase I compared with free DNA, and that the model drug (camptothecin) released exhibits similar efficacy as free, unmodified drugs toward cancer cells.

In recent years, it has been demonstrated that specific arrangements of nucleic acids into unique three-dimensional architectures can give rise to unusual properties absent for linear or circular forms of the nucleic acid.[1−9] For example, spherical nucleic acids (SNAs), which are typically comprised of a dense DNA shell surrounding a gold nanoparticle core, show high levels of cellular uptake,[10] enhanced binding with complementary strands,[11] and increased DNA stability against enzymatic degradation.[12] These properties have been shown to result from the packing and orientation of the oligonucleotides on the surface of the gold nanoparticles, and are not directly related to the metallic core.[13] Indeed, SNAs with different core compositions (polymers,[14] lipids,[15] silica,[16] metal oxides,[17] and quantum dots[18]) or even those lacking a core[12] all exhibit similar physiochemical and biological properties. Thus, through arrangement of the DNA strands, many problems associated with nucleic acid delivery, especially co-carrier-induced cytotoxicity and immunogenicity,[19] can be bypassed.

The rapid endocytosis of SNAs also makes them suitable for delivery applications.[20−22] It is hypothesized that the co-delivery of nucleic acids and small molecule drugs can allow one to independently access gene and protein targets, thereby circumventing drug resistance, which one-dimensional therapeutic strategies cannot address.[23] Payload molecules such as platinum(IV) prodrugs[24] and doxorubicin[25] have been delivered to cells via covalent attachment to either the terminus of the oligonucleotides or the gold nanoparticle surface. In these systems, however, the cores of the nanoparticles do not play a significant role but contribute to a nonbioresorbable metallic mass. Naturally, for applications where the gold core is not utilized, it is advantageous to convert the core to a reservoir for payload molecules. Herein, we construct and test a drug-cored nucleic acid nanostructure containing hydrophobic chemotherapeutic agents. Such carrier-free, single entity agent retains many of the unique properties of the SNA while offering benefits including precise drug loading ratio,[26] improved drug solubility,[27,28] and spatiotemporally controlled release.[29]

To create a drug core, we designed and synthesized a DNA−camptothecin (CPT) amphiphile (Scheme 1). It consists of three CPT molecules connected to a phenol-based self-immolative linker. The phenol group is capped with a photolabile 2-nitrobenzyl ether moiety, to which DNA strands are attached. The amphiphilicity of the DNA−CPT conjugate allows it to assemble into micellar nanostructures (of different morphologies, depending on DNA size and assembly condition, vide infra) in an aqueous environment. The 2-nitrobenzyl group can be cleaved by UV light (365 nm) or via a two-photon mechanism,[30,31] releasing the DNA from the nanostructure and leaving a decapped self-immolative drug core, which can then rapidly undergo a spontaneous and irreversible degradation process,[32] to generate free CPT molecules. We expect this method to be relatively general

Scheme 1. Schematics of the DNA−Drug Nanostructures Assembled from Photolabile DNA−Drug Amphiphiles

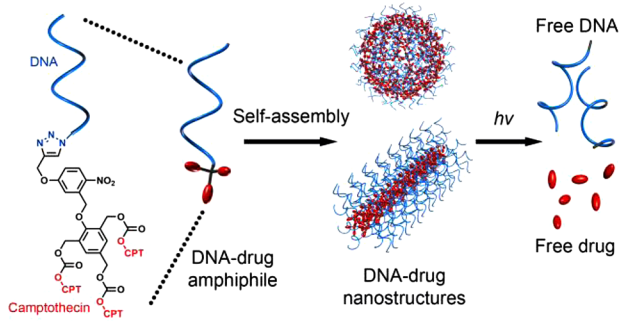

Received: January 23, 2015
Published: April 29, 2015

DOI: 10.1021/jacs.5b00795
J. Am. Chem. Soc. 2015, 137, 6112−6115

with regard to the kind of drug molecules because many chemotherapeutic drugs are hydrophobic.

The successful synthesis of the linker is confirmed by Matrix-Assisted Laser Desorption Ionization-Time of Flight Mass Spectrometry (MALDI-ToF MS, 395.0 Da $[M + Na]^+$, calc. 396.1 Da), NMR, and IR (Figures S1–S2). CPT molecules are attached to the linker by forming carbonate linkages between the CPT 4-hydroxyl group and the linker's three benzyl alcohol groups. Although singly and doubly modified linkers are formed, the yield for the triply modified linker (linker–CPT_3) is satisfactory (ca. 30%), and impurities can be easily removed by HPLC. The mass of the product is determined by MALDI-ToF MS (m/z = 1518.9 Da $[M + Na]^+$, calc. 1518.4 Da, Figure S3). Next, azide-modified DNA strands of various lengths (5, 9, 13, 17, and 20 bases, Table S1) are attached to linker–CPT_3 by Cu(I)-catalyzed click chemistry, followed by HPLC purification. The DNA strand with 20 bases (DNA_{20}) is labeled with a Cy3 dye at the 3′ end to enable tracking by fluorescence and UV–vis spectroscopy. The UV–vis spectrum of the DNA_{20}–CPT conjugate shows three absorption maxima at 260, 370, and 551 nm, which are indicative of the presence of DNA, CPT, and Cy3, respectively (Figure S4). The molar ratio of CPT: Cy3 is calculated based on free CPT and Cy3 extinction coefficients (19.9 and 136 L $mmol^{-1}$ cm^{-1}) to be 3.4:1, which is close to 3:1. The conjugate is also characterized by agarose gel electrophoresis (Figure 1A). Multiplex gel imaging (Cy3 and Cy2 excitation/emission filters applied) shows a single band emitting both Cy3 (green) and CPT (red) fluorescence. These results indicate that the DNA–CPT conjugate is successfully synthesized and purified. The molecular purity of the conjugate ensures a constant DNA:drug molar ratio, which is important for consistency in drug formulation and efficacy.[33] In addition, the conjugate can mask the toxicity of the chemotherapeutic agent before it is released at targeted site by light triggering.

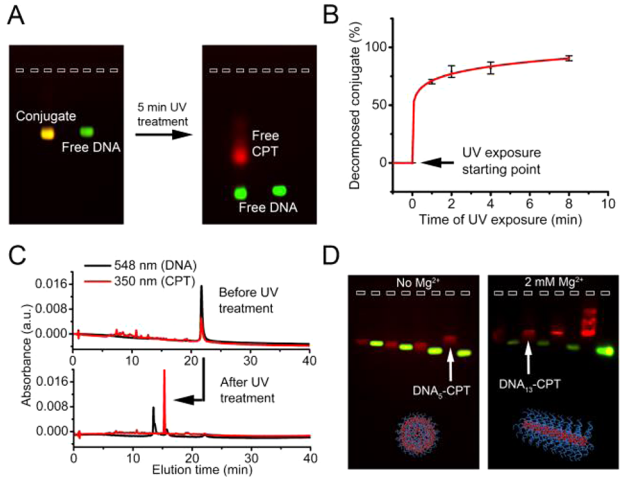

Figure 1. (A) Multiplex gel images of the DNA_{20}–CPT conjugate and free Cy3–DNA_{20} (1% agarose, 0.5× TBE) before (left) and after (right) UV treatment. The top of the gel lanes is marked with a dashed line. (B) Release kinetics of the DNA_{20}–CPT conjugate as a function of light exposure times (365 nm, 10 $mJ{\cdot}s^{-1}{\cdot}cm^{-2}$). (C) Reverse-phase HPLC chromatograms of the DNA_{20}–CPT conjugate before (top) and after (bottom) light exposure, showing the conjugate peak splitting into two, which match the elution times of free DNA and CPT. (D) Multiplex gel images (5% agarose, 0.05× PBS) of DNA–drug conjugates (red) or free DNA (green) in the absence (left) or presence (right) of 2 mM Mg^{2+}. The top of the gel lanes is marked with a dashed line. From left to right: DNA_{17}–CPT, DNA_{16F}, DNA_{13}–CPT, DNA_{12F}, DNA_9–CPT, DNA_{8F}, DNA_5–CPT, and DNA_{4F}.

The photocleavage and self-immolation reactions are visualized by gel electrophoresis. The DNA_{20}–CPT conjugate is first electrophoresed for 30 min (free Cy3–DNA_{20} used as a control), and thereafter UV light (365 nm, 10 $mJ{\cdot}s^{-1}{\cdot}cm^{-2}$) is applied for 5 min, followed by another 30 min of electrophoresis. After the initial run, the conjugate shows nearly the same migration distance as the free Cy3–DNA_{20} strand (Figure 1A). However, UV treatment causes the conjugate to split into two bands: a green band, which traveled the same overall distance as the free Cy3–DNA_{20}, and a broad, slower-migrating red band, which correlates with free CPT.

To determine the kinetics of the payload release, we used reverse-phase HPLC to monitor the extent of drug and DNA released as a function of UV exposure times. Without UV exposure, a single peak was observed at both Cy3 (548 nm) and CPT (350 nm) channels. With only 1 min of UV irradiation (365 nm, 10 $mJ{\cdot}s^{-1}{\cdot}cm^{-2}$), ca. 73% of the conjugate is cleaved, but to reach >90% cleavage, 8 min of light irradiation is required (Figure 1B). Two new peaks are observed following UV treatment, and their elution times match that of free CPT and DNA (Figures 1C, S5). MALDI-ToF MS also confirms that the DNA_{20} released gains an extra ca. 190 Da of mass compared with the free azide–Cy3–DNA_{20}, which is mass of the phenyl aldehyde residue of the cleaved linker. Of note, we did not observe a two-stage release profile, i.e., DNA released first followed by CPT, despite the fact that the release of free CPT requires an additional step (the self-immolation process, Scheme S3). It is likely that the time scale of the HPLC analysis is much longer than that of the self-immolation reaction.

Next, we investigated how the DNA–CPT conjugates can self-assemble to form micellar nanostructures in solution. Agarose gel electrophoresis (5%, 0.05× PBS buffer) of the DNA_5–CPT conjugate shows a sharp band corresponding to a much higher MW compared with free DNA_5, which indicates the formation of self-assembled structures (Figure 1D). The number-average hydrodynamic diameter ($D_{h(n)}$) of the nanostructure is 32 ± 13 nm as determined by Dynamic Light Scattering (DLS, Figure S8). Transmission Electron Microscopy (TEM) shows that the DNA_5–CPT conjugate assembled into a spherical morphology with a dry-state diameter of 28 ± 5 nm (Figure 2A). The MW of the aggregates decreases with increasing DNA length, presumably due to reduced aggregation numbers resulting from increased amphiphile headgroup volume. When the DNA strand is longer than 9 bases, the migration rate of the conjugate becomes

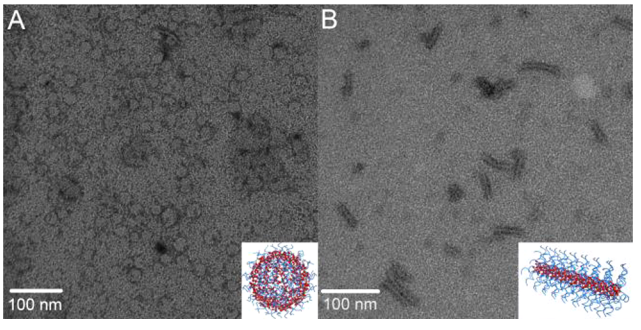

Figure 2. TEM images (stained by 2% uranyl acetate) of (A) the DNA_5–CPT conjugate prepared from PBS buffer, and (B) the DNA_{20}–CPT conjugate prepared from PBS buffer with 5 mM $MgCl_2$.

DOI: 10.1021/jacs.5b00795
J. Am. Chem. Soc. 2015, 137, 6112–6115

identical to that of free DNA, which indicates that micelle formation is no longer thermodynamically favorable. However, in the presence of 2–5 mM divalent Mg^{2+} ion, which is within the physiological range for Mg^{2+} concentration,[34] self-assembly takes place even for DNA_{20}–CPT (longest DNA tested), as indicated by agarose gel electrophoresis (Figure S9). This is likely because divalent Mg^{2+} ions are able to bind with the charged DNA phosphate groups and bridge different strands, and thereby attenuate the entropy penalty to form higher order, densely packed DNA nanostructures. Interestingly, the mode of packing for the DNA_{20}–CPT conjugate is different from that of smaller conjugates. The hydrodynamic diameter ($D_{h(n)}$) of the assembled structure is 22 ± 8 nm as determined by DLS (Figure S8). TEM reveals that rod-like nanostructures have formed. The rods appear to be relatively rigid, with length on the order of ca. 53 ± 14 nm and cross-section diameter approximately 8 ± 1 nm (Figure 2B). It is possible that the rods are formed by stacking circularly arranged DNA_{20}–CPT conjugates in a vertical fashion, which results a cylindrical morphology.[35] The fact that longer hydrophilic segments give rise to rod-like structures appears to be against the common rules of amphiphilic block copolymer assembly; however, tunable attractive interactions mediated by ions between the hydrophilic segments of different chains are oftentimes ignored in canonical theories.[36,37] Nonetheless, these morphological results are preliminary, and additional characterization is needed to fully rule out artifacts resulting from TEM sample preparation and imaging. Accordingly, a more detailed self-assembly study is planned.

A hallmark feature for SNAs is their resistance to nuclease degradation. This property stems from the high local sodium ion concentration and steric inaccessibility to the enzyme.[38] It is of interest to study whether the packing of the DNA–CPT conjugate can also lower the rate of DNA degradation by nucleases. Because nucleic acid sequences with a length of 18–25 bases are particularly useful for gene regulation applications,[39] we focused on the DNA_{20}–CPT conjugate. We synthesized a dabcyl-modified complementary strand for DNA_{20}–CPT, and hybridized it to preformed, Cy3-modified DNA_{20}–CPT nanostructure. The dabcyl quencher quenches the fluorescence of Cy3 when the duplex is formed. Upon introduction of DNase I (a nuclease with preference for phosphodiester linkages adjacent to pyrimidine nucleotides), the Cy3 fluorophores are released and an increase in fluorescence can be observed (Figure 3A). We found that the initial rate of duplex degradation for the DNA_{20}–CPT nanostructures is approximately 60% of that for the free duplexes, and the time needed for half degradation is ca. 4.5 times longer (Figure 3B).

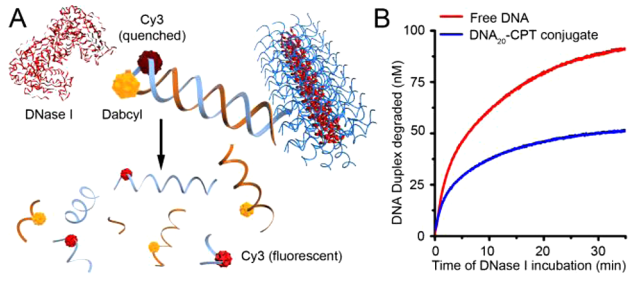

Figure 3. (A) Schematic of the DNA stability assay against DNase I. (B) Kinetics of the enzymatic degradation of DNA_{20}–CPT and free Cy3–DNA_{20} duplexes (100 nM), expressed as percent Cy3 fluorescence as a function of time upon DNase I introduction.

After establishing that the DNA–drug nanostructures exhibit SNA-like properties, we next characterized these nanostructures in vitro for light-activated cytotoxicity, using the breast cancer cell line SK-BR-3 as a model system. Confocal microscopy confirmed that DNA_{20}–CPT nanostructures can be taken up by SK-BR-3 cells following 6 h of incubation (1 μM) (Figure 4A). To assess the efficacy of the DNA–drug nanostructure, we

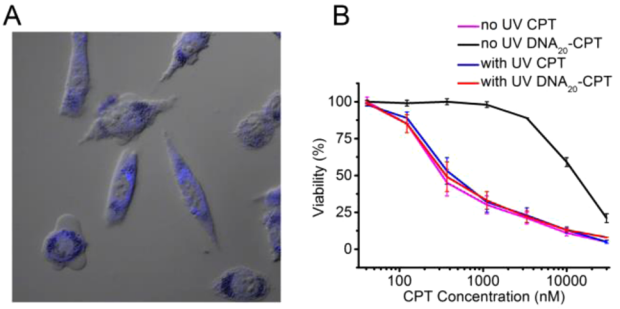

Figure 4. (A) Confocal microscopy image of SK-BR-3 cells following incubation with DNA_{20}–CPT nanostructures (1 μM) for 6 h (CPT channel). (B) Cytotoxicity measurement of CPT and DNA_{20}–CPT nanoparticles in the absence and presence of UV. Error bars denote standard error of mean from three independent experiments.

first determined the proper dosage of UV light to minimize UV-induced cell death. SK-BR-3 cells were irradiated with 0.5–4.5 min of UV light (365 nm, 10 $mJ \cdot s^{-1} \cdot cm^{-2}$) in the absence of drug, and cell viability assays were carried out after 24 h (Figure S10). Under these conditions, photocytotoxicity is undetectable (cell viability near 100%). We next investigated whether a non-cell-killing dose of UV light can activate the cytotoxicity of the DNA–drug nanostructure. SK-BR-3 cells were first treated with DNA_{20}–CPT or free CPT, and after 6 h, UV light was applied. Non-UV-treated cells were used as controls. Because some extent of cell uptake has occurred within the initial 6 h of drug treatment, the CPT is expected to be released both intracellularly and extracellularly. The DNA_{20}–CPT exhibited much reduced toxicity compared with free CPT in the absence of UV light (IC_{50} 13 μM vs 330 nM), as expected from the chemical modification and packing of CPT (Figure 4B). Furthermore, the addition of UV irradiation did not increase the cytotoxicity of free CPT. On the other hand, the cell-killing efficacy of the DNA_{20}–CPT conjugate was significantly amplified by UV treatment, which resulted in similar levels of toxicity as that of free CPT control (IC_{50} 360 nM). These results suggest that the DNA–CPT conjugates can achieve controlled cytotoxicity by light triggering.

In summary, we have demonstrated that nucleic acid/drug nanostructures can be achieved by taking advantage of the amphiphilicity of nucleic acid–drug conjugates. The nanostructures resulting from the solution assembly exhibit unique properties often found with densely arranged nucleic acid nanostructures, such as rapid cell uptake and enhanced nuclease stability, which makes these structures suitable as carrier-free delivery platforms. Furthermore, the photolabile DNA–CPT nanostructures show localized, light-controlled cytotoxicity, providing a favorable therapeutic window for potential clinical applications.

DOI: 10.1021/jacs.5b00795
J. Am. Chem. Soc. 2015, 137, 6112–6115

■ ASSOCIATED CONTENT

Supporting Information

Materials and methods, additional characterization data. The Supporting Information is available free of charge on the ACS Publications website at DOI: 10.1021/jacs.5b00795.

■ AUTHOR INFORMATION

Corresponding Author

*k.zhang@neu.edu

Notes

The authors declare no competing financial interest.

■ ACKNOWLEDGMENTS

The authors thank William Fowle at the NEU Biology Department for help with the TEM. Financial support from Northeastern University start-up, NEU-DFCI seed grant, and NSF CAREER award (1453255) is gratefully acknowledged.

■ REFERENCES

(1) Walsh, A. S.; Yin, H.; Erben, C. M.; Wood, M. J.; Turberfield, A. J. *ACS Nano* **2011**, *5*, 5427.
(2) Rush, A. M.; Thompson, M. P.; Tatro, E. T.; Gianneschi, N. C. *ACS Nano* **2013**, *7*, 1379.
(3) Zheng, J.; Zhu, G.; Li, Y.; Li, C.; You, M.; Chen, T.; Song, E.; Yang, R.; Tan, W. *ACS Nano* **2013**, *7*, 6545.
(4) Conway, J. W.; Madwar, C.; Edwardson, T. G.; McLaughlin, C. K.; Fahkoury, J.; Lennox, R. B.; Sleiman, H. F. *J. Am. Chem. Soc.* **2014**, *136*, 12987.
(5) Lu, X.; Watts, E.; Jia, F.; Tan, X.; Zhang, K. *J. Am. Chem. Soc.* **2014**, *136*, 10214.
(6) Lin, C.; Jungmann, R.; Leifer, A. M.; Li, C.; Levner, D.; Church, G. M.; Shih, W. M.; Yin, P. *Nat. Chem.* **2012**, *4*, 832.
(7) Tian, C.; Li, X.; Liu, Z.; Jiang, W.; Wang, G.; Mao, C. *Angew. Chem., Int. Ed.* **2014**, *53*, 8041.
(8) Lau, K. L.; Hamblin, G. D.; Sleiman, H. F. *Small* **2014**, *10*, 660.
(9) Zhang, K.; Zhu, X.; Jia, F.; Auyeung, E.; Mirkin, C. A. *J. Am. Chem. Soc.* **2013**, *135*, 14102.
(10) Giljohann, D. A.; Seferos, D. S.; Patel, P. C.; Millstone, J. E.; Rosi, N. L.; Mirkin, C. A. *Nano Lett.* **2007**, *7*, 3818.
(11) Lytton-Jean, A. K.; Mirkin, C. A. *J. Am. Chem. Soc.* **2005**, *127*, 12754.
(12) Cutler, J. I.; Zhang, K.; Zheng, D.; Auyeung, E.; Prigodich, A. E.; Mirkin, C. A. *J. Am. Chem. Soc.* **2011**, *133*, 9254.
(13) Cutler, J. I.; Auyeung, E.; Mirkin, C. A. *J. Am. Chem. Soc.* **2012**, *134*, 1376.
(14) Chen, X. J.; Sanchez-Gaytan, B. L.; Hayik, S. E. N.; Fryd, M.; Wayland, B. B.; Park, S. J. *Small* **2010**, *6*, 2256.
(15) Banga, R. J.; Chernyak, N.; Narayan, S. P.; Nguyen, S. T.; Mirkin, C. A. *J. Am. Chem. Soc.* **2014**, *136*, 9866.
(16) Young, K. L.; Scott, A. W.; Hao, L.; Mirkin, S. E.; Liu, G.; Mirkin, C. A. *Nano Lett.* **2012**, *12*, 3867.
(17) Zhang, C.; Macfarlane, R. J.; Young, K. L.; Choi, C. H.; Hao, L.; Auyeung, E.; Liu, G.; Zhou, X.; Mirkin, C. A. *Nat. Mater.* **2013**, *12*, 741.
(18) Wu, X. A.; Choi, C. H.; Zhang, C.; Hao, L.; Mirkin, C. A. *J. Am. Chem. Soc.* **2014**, *136*, 7726.
(19) Ibricevic, A.; Guntsen, S. P.; Zhang, K.; Shrestha, R.; Liu, Y.; Sun, J. Y.; Welch, M. J.; Wooley, K. L.; Brody, S. L. *Nanomed. Nanotechnol. Biol. Med.* **2013**, *9*, 912.
(20) Patel, P. C.; Giljohann, D. A.; Daniel, W. L.; Zheng, D.; Prigodich, A. E.; Mirkin, C. A. *Bioconjugate Chem.* **2010**, *21*, 2250.
(21) Choi, C. H.; Hao, L.; Narayan, S. P.; Auyeung, E.; Mirkin, C. A. *Proc. Natl. Acad. Sci. U.S.A.* **2013**, *110*, 7625.
(22) Hamblin, G. D.; Carneiro, K. M. M.; Fakhoury, J. F.; Bujold, K. E.; Sleiman, H. F. *J. Am. Chem. Soc.* **2012**, *134*, 2888.
(23) Wang, Y.; Gao, S.; Ye, W. H.; Yoon, H. S.; Yang, Y. Y. *Nat. Mater.* **2006**, *5*, 791.
(24) Dhar, S.; Daniel, W. L.; Giljohann, D. A.; Mirkin, C. A.; Lippard, S. J. *J. Am. Chem. Soc.* **2009**, *131*, 14652.
(25) Alexander, C. M.; Hamner, K. L.; Maye, M. M.; Dabrowiak, J. C. *Bioconjugate Chem.* **2014**, *25*, 1261.
(26) Cheetham, A. G.; Zhang, P.; Lin, Y. A.; Lock, L. L.; Cui, H. *J. Am. Chem. Soc.* **2013**, *135*, 2907.
(27) Larson, N.; Ghandehari, H. *Chem. Mater.* **2012**, *24*, 840.
(28) Duncan, R. *Nat. Rev. Cancer* **2006**, *6*, 688.
(29) Chan, J. M.; Zhang, L.; Tong, R.; Ghosh, D.; Gao, W.; Liao, G.; Yuet, K. P.; Gray, D.; Rhee, J. W.; Cheng, J.; Golomb, G.; Libby, P.; Langer, R.; Farokhzad, O. C. *Proc. Natl. Acad. Sci. U.S.A.* **2010**, *107*, 2213.
(30) Pelliccioli, A. P.; Wirz, J. *Photochem. Photobiol. Sci.* **2002**, *1*, 441.
(31) McKinnon, D. D.; Brown, T. E.; Kyburz, K. A.; Kiyotake, E.; Anseth, K. S. *Biomacromolecules* **2014**, *15*, 2808.
(32) Haba, K.; Popkov, M.; Shamis, M.; Lerner, R. A.; Barbas, C. F., 3rd; Shabat, D. *Angew. Chem., Int. Ed.* **2005**, *44*, 716.
(33) Chen, Z. P.; Zhang, P. C.; Cheetham, A. G.; Moon, J. H.; Moxley, J. W.; Lin, Y. A.; Cui, H. *J. Controlled Release* **2014**, *191*, 123.
(34) Swaminathan, R. *Clin. Biochem. Rev.* **2003**, *24*, 47.
(35) Lin, Y. A.; Cheetham, A. G.; Zhang, P.; Ou, Y. C.; Li, Y.; Liu, G.; Hermida-Merino, D.; Hamley, I. W.; Cui, H. *ACS Nano* **2014**, *8*, 12690.
(36) Mai, Y. Y.; Eisenberg, A. *Chem. Soc. Rev.* **2012**, *41*, 5969.
(37) Borisov, O. V.; Zhulina, E. B. *Macromolecules* **2002**, *35*, 4472.
(38) Seferos, D. S.; Prigodich, A. E.; Giljohann, D. A.; Patel, P. C.; Mirkin, C. A. *Nano Lett.* **2009**, *9*, 308.
(39) He, L.; Hannon, G. J. *Nat. Rev. Genet.* **2004**, *5*, 522.

DOI: 10.1021/jacs.5b00795
J. Am. Chem. Soc. 2015, 137, 6112−6115